Understanding global monsoon precipitation changes during the 8.2 ka event and the current warm period

Article *in* Palaeogeography Palaeoclimatology Palaeoecology · November 2021

DOI: 10.1016/j.palaeo.2021.110757

CITATIONS
0

READS
31

4 authors:

Peng He
Nanjing Normal University
2 PUBLICATIONS **0** CITATIONS
SEE PROFILE

Jian Liu
Chinese Academy of Sciences
68 PUBLICATIONS **1,855** CITATIONS
SEE PROFILE

Bin Wang
University of Hawai'i at Mānoa
393 PUBLICATIONS **31,743** CITATIONS
SEE PROFILE

Weiyi Sun
Nanjing Normal University
26 PUBLICATIONS **220** CITATIONS
SEE PROFILE

Palaeogeography, Palaeoclimatology, Palaeoecology xxx (xxxx) xxx

Contents lists available at ScienceDirect

Palaeogeography, Palaeoclimatology, Palaeoecology

journal homepage: www.elsevier.com/locate/palaeo

Understanding global monsoon precipitation changes during the 8.2 ka event and the current warm period

Peng He [a], Jian Liu [a,b,c,*], Bin Wang [d,e], Weiyi Sun [a]

[a] Key Laboratory for Virtual Geographic Environment, Ministry of Education, State Key Laboratory Cultivation Base of Geographical Environment Evolution of Jiangsu Province, Jiangsu Center for Collaborative Innovation in Geographical Information Resource Development and Application, School of Geography Science, Nanjing Normal University, Nanjing 210023, China

[b] Jiangsu Provincial Key Laboratory for Numerical Simulation of Large-Scale Complex Systems, School of Mathematical Science, Nanjing Normal University, Nanjing 210023, China

[c] Open Studio for the Simulation of Ocean-Climate-Isotope, Qingdao National Laboratory for Marine Science and Technology, Qingdao 266237, China

[d] Department of Atmospheric Sciences and International Pacific Research Center, School of Ocean Earth Science and Technology, University of Hawaii, Honolulu, HI 96822, USA

[e] Key Laboratory of Meteorological Disaster of Ministry of Education and Earth System Modeling Center, Nanjing University of Information Science and Technology, Nanjing 210044, China

ARTICLE INFO

Editor: Paul Hesse

Keywords:
Holocene
8.2 ka event
Global monsoon precipitation
TraCE-21 ka simulation
External forcing
Current warm period

ABSTRACT

Global monsoon (GM) precipitation has profound impacts on water resources, food security, and the livelihood of about two-thirds of the world's population. Understanding the contrasting changes of GM precipitation (GMP) during the 8.2 ka cold event and the present-day warm event helps better comprehend the common origin of the GMP change and its future projection. We analyzed a suite of transient climate evolutions (TraCE-21 ka simulation). We show that the simulated monsoon rainfall changes during the 8.2 ka abrupt cooling event are qualitatively consistent with the paleoclimate archive collected worldwide. The simulated Northern Hemisphere monsoon (NHM) precipitation significantly decreased by 12.4% per one degree of global mean temperature change (12.4%/°C) while the Southern Hemisphere monsoon (SHM) precipitation increased by 4.2%/°C. The cooling-induced suppressed upward motion plays a dominant role in reducing NHM precipitation, and the reduced moisture adds to the circulation effect, whereas the enhanced SHM precipitation is mainly due to the moisture increase. In the 8.2 ka event, the circulation response reinforces the moisture-induced drought over the NHM region, resulting in an excessive precipitation sensitivity to temperature change (12.4%/°C). In contrast, during the present warm period, the greenhouse warming-induced moisture and circulation effects cancel each other, resulting in a moderate sensitivity (1.8%/°C). Although meltwater and greenhouse gas forcings induce contrasting global temperature change patterns, the GMP changes are governed by common root causes: forced NH-SH thermal contrast, land-ocean thermal contrast, and the tropical SST gradients. The moisture change plays a crucial role in altering precipitation amount but not spatial distribution. We suggest that the external forcing-induced warming (cooling) pattern drives the circulation changes (dynamic effects), determining the spatial structure of the monsoon rainfall change in the past, present, and future.

1. Introduction

Monsoon is essentially a forced response of the earth's climate system to annual variation of insolation, thus a global phenomenon (Wang et al., 2012). The global monsoon (GM) is a dominant mode of the annual variation in tropical and subtropical precipitation and circulation (Wang and Ding, 2008). Global monsoon precipitation (GMP) plays an important role in the global energy and water cycle. GMP imposes a direct and significant impact on the lives of two-thirds of the world's population and vegetation (An et al., 2015; Wang et al., 2012). Therefore, study of GMP changes have profound scientific and socio-economic significance.

* Corresponding author at: Key Laboratory for Virtual Geographic Environment, Ministry of Education, State Key Laboratory Cultivation Base of Geographical Environment Evolution of Jiangsu Province, Jiangsu Center for Collaborative Innovation in Geographical Information Resource Development and Application, School of Geography Science, Nanjing Normal University, Nanjing 210023, China.
E-mail address: jliu@njnu.edu.cn (J. Liu).

https://doi.org/10.1016/j.palaeo.2021.110757
Received 8 June 2021; Received in revised form 15 September 2021; Accepted 8 November 2021
Available online 14 November 2021

The GMP displays multi-scale variations induced by internal feedback processes and external forcings. The inter-annual to multi-decadal variation of GMP is mainly caused by El Niño-Southern Oscillation (ENSO), and the Atlantic Multidecadal Oscillation (AMO) (Wang et al., 2012, 2013). Liu et al. (2009a) investigated the response and mechanisms of GMP to natural and anthropogenic forcing during the last millennium. They found that increased NH monsoon precipitation (NHMP) is linked to the enhanced NH land-ocean thermal contrast and NH-Southern Hemisphere (SH) thermal contrast. The NHMP responds more sensitively to the greenhouse gas (GHG) than to the solar-volcanic radiative forcing, but the SH monsoon precipitation (SHMP) responds to the solar-volcanic radiative forcing more sensitively than the NHMP (Liu et al., 2012). Chai et al. (2018) argued that the volcanic forcing is more effective to GMP change than the solar and GHG forcing due to the common drivers of monsoon moisture and circulation. The GMP changes under the current warm period (CWP) have been investigated using the models. The GHGs' radiation forcing induces a warm NH relative to the SH, which favors an enhanced interhemispheric thermal contrast due to more substantial warming over the land than over the ocean, thus increasing the GM strength and extent (D'Agostino et al., 2019; Acosta Navarro et al., 2017). On the hemispheric scale, evaluation of Coupled Model Intercomparison Phase 6 (CMIP6) simulations has indicated a wetter NHMP and an insignificant change of the SHMP (Wang et al., 2020).

With future warming accelerates more rapidly, increased melting of the ice sheet might trigger abrupt cooling events (Liu et al., 2017; Rahmstorf et al., 2015; Srokosz and Bryden, 2015). How will GMP change if GHG continues to increase and meltwater flux is enhanced? Understanding of GMP responses to individual natural variability caused by meltwater and anthropogenic GHG is crucial to answering this question. It is important to investigate the sensitivity of GMP responses to the two different types of forcing, not only for deepening our understanding of the mechanisms of GMP change but also for distinguishing the precipitation sensitivity to global temperature variability between the natural and anthropogenic forcing. Under a situation with larger sensitivity, the eco-environmental change in monsoon regions may rely more on precipitation than on temperature (Cheng et al., 2019).

The Holocene is the most recent interglacial period when the precession orbital forcing moves through a complete half cycle and the ice sheets retreat. Abrupt climate change events have been found in the North Atlantic drift ice records throughout the Holocene (O'Brien et al., 1995; Andrews et al., 1997; Bond, 1997). Many researchers have been motivated to investigate the Holocene abrupt climate changes due to the concern that similar rapid-climate shifts may reappear in the future (Alley et al., 2003; Holmes et al., 2011; Park et al., 2019). The most prominent Holocene abrupt climate change events in the Northern Hemisphere (NH) occurred between 8.5 and 7.9 ka, termed "the 8.2 ka event" (Alley et al., 1997; Renssen et al., 2001; Alley and Agustsdottir, 2005; Morrill et al., 2013; Matero et al., 2017). This abrupt climate event serves as a stratigraphic marker between the Early and Middle Holocene (Finkenbinder et al., 2016; Walker et al., 2018). The 8.2 ka event is characterized by the cooling in the North Atlantic and surrounding regions (Bauer and Ganopolski, 2004; Morrill et al., 2013; Wagner et al., 2013; Morrill and Jacobsen, 2005). A slowdown of the Atlantic Meridional Overturning Circulation (AMOC) due to freshwater injection has been proposed to cause the 8.2 ka event (Barber et al., 1999). Several climate modeling studies indicated that this event was forced by the drainage of proglacial Lake Agassiz-Ojibway into the Hudson Bay (Clarke et al., 2004). These modeling works reproduced the patterns of the climate response to the meltwater injection, which include North Atlantic cooling and a southward shift of the Intertropical Convergence Zone (ITCZ) (Wiersma et al., 2006; Matero et al., 2017). The 8.2 ka event provides an opportunity for studying the impact of meltwater on GMP.

Abrupt hydrological changes around 8.2 ka have been documented in various individual monsoon regions. Decreased precipitation was recorded in the Asian monsoon (Wang et al., 2005; Cheng et al., 2009; Dixit et al., 2014; Tan et al., 2020), North American monsoon (Lachniet et al., 2013; Winter et al., 2020), and North African monsoon (Weldeab et al., 2014; Tierney et al., 2017b) regions, whereas the wetter tendency was detected in South America (Cheng et al., 2009), northern Australian (Ayliffe et al., 2013; Denniston et al., 2017), and Madagascar (Voarintsoa et al., 2019). Previous studies on the change of monsoon precipitation are mostly focused on regional monsoons. However, the energy and water vapor are conserved only on the global scale (Trenberth et al., 2000). Investigation of monsoon precipitation change from a global perspective is necessary and advantageous. The changes of global monsoon precipitation and the physical mechanisms during the 8.2 ka event have not been explored.

This study aims to understand the mechanisms governing the GMP change during the 8.2 ka event in comparison with the GMP change in the CWP. Specifically, we address the following questions: What are the temporal and spatial characteristics of GMP change during the 8.2 ka event? What physical process and mechanism govern the GMP change during the 8.2 ka event and CWP? To answer these questions, we use the model simulated result from the TraCE-21 ka project. The data and method are introduced in Sec. 2. The results are shown in Sect.3. Section 4 discussed possible physical processes behind the GMP changes during the 8.2 ka event and CWP. Section 5 presents a summary.

2. Data and methods

2.1. Model data

The model data used in this study are from the simulations of transient climate evolution over the last 21 ka ("TraCE-21 ka") (Liu et al., 2009b; He et al., 2013). The simulation used version 3 of the Community Climate System Model (CCSM3), which consists of the Community Atmospheric Model version 3 (CAM3) with a horizontal resolution of T31 (about 3.75° × 3.75°) and the Parallel Ocean Program (POP) ocean model. The ocean model has a longitudinal resolution of 3.6° and a variable latitudinal resolution from about 0.9° near the equator to a coarser resolution poleward.

The TraCE-21 ka experiments designs are lighted in Table 1. The transient experiment with all forcing (TraCE-AF) is forced by the transient variations of orbital (ORB) configuration (Berger, 1978), GHG concentrations (Joos and Spahni, 2008), meltwater fluxes (MWF) (Liu et al., 2009b), and ice sheet (ICE) topography and extent (Peltier, 2004). In addition, four single-forcing experiments were conducted. They are forced by only one of the forcings in the TraCE-AF experiment: TraCE-ORB, TraCE-GHG, TraCE-MWF, and TraCE-ICE. The time series of external forcings used in the TraCE-21 ka experiments are shown in Fig. 1. The meltwater flux injection into NH oceans is based on a specific time slice (e.g., 9.0 ka into the Arctic, St. Lawrence, and Hudson Strait). In the TraCE-ORB and TraCE-GHG experiment, the other forcings are fixed at the state at 22 ka. In the TraCE-MWF and TraCE-ICE experiment, the other forcings were held fixed at the state of 19 ka. A detailed description of the TraCE-21 ka experiment design is referred to He (2011) and He et al. (2013).

The TraCE-AF simulation is compared with proxy data. It can

Table 1
The TraCE-21 ka experiments design: the all forcing experiment and four single-forcing experiments.

	Orbital	GHG	Meltwater	Ice sheet	Time span
TraCE-AF	Transient	Transient	Transient	Transient	22–0 ka
TraCE-ORB	Transient	–	–	–	22–0 ka
TraCE-GHG	–	Transient	–	–	22–0 ka
TraCE-MWF	–	–	Transient	–	19–0 ka
TraCE-ICE	–	–		Transient	19–0 ka

The em dash represents that the forcing is fixed at the beginning of the corresponding experiment.

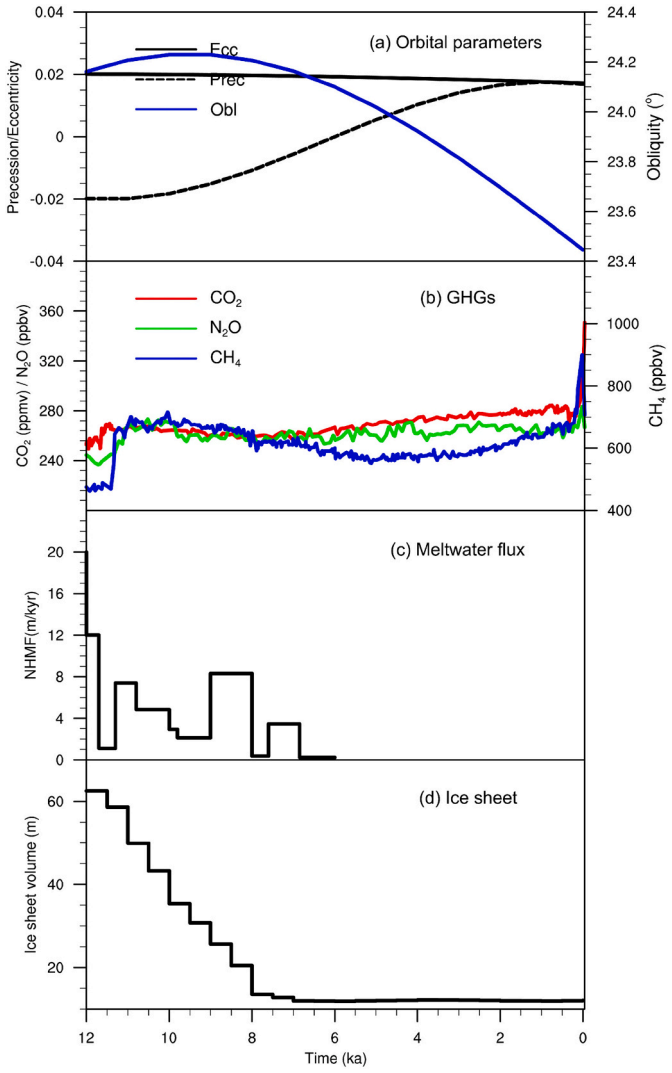

Fig. 1. External Forcing used in TraCE-21 ka experiment. Time series are (a) Orbital parameters, including, eccentricity (Ecc), precession (Prec) and obliquity (Obl) (Berger, 1978), (b) GHGs (Joos and Spahni, 2008), (c) Meltwater flux into the Northern Hemisphere Ocean (Liu et al., 2009b) (expressed as sea-level change in meters per 1000 years) and (d) Ice Sheets (Peltier, 2004) (expressed as mean ice sheet thickness).

reproduce major features of the climate evolution during the last 21 ka (Clark et al., 2012; Shakun et al., 2012). It has been used to explain the mechanism of climate change since the Last Glacial Maximum (LGM), such as the Bølling-Allerød warming (Liu et al., 2009b), the Asian-African monsoon evolution over the past 21 kyr (Shi and Yan, 2019), the East Asian summer and winter monsoon relationship across different timescales in Holocene (Yan et al., 2020). In the present work, we use the TraCE-21 ka experiment results to compare the GM precipitation changes in 8.2 ka and CWP.

2.2. Identification of 8.2 ka event and CWP in the TraCE-21 ka simulation

The decadal mean NH surface temperature during the 9.8–7.8 ka shows a multi-centennial cooling from 8.5–8.0 ka (Fig. 2a), which indicates that the simulated abrupt change event is potentially comparable to the 8.2 ka event. Therefore, we selected the warmest 200-yr (9.2–9.0 ka) before the injection of freshwater as the warm centennial period and the coldest 200-yr (8.2–8.0 ka) after the injection of freshwater as the cold centennial period to identify the spatial patterns of the GMP change (Fig. 2a). For comparison, we defined the difference between the present-day (1940–1990) and pre-industrial period (1830–1880) to represent the CWP change (Fig. 2b).

2.3. Observation and proxy data

The Climate Merged Analysis of Precipitation (CMAP) data (Xie and Arkin, 1997) and the Global Precipitation Climatology Project (GPCP) version 2.3 data (Adler et al., 2018) from 1979 to 2008 are merged by the arithmetic mean to serve as the observation data (Lee and Wang, 2014; Yan et al., 2016). To reveal the hydroclimate response to the 8.2 ka event over monsoon regions, we also collected previously published proxy data from 47 sites based on several criteria (Table 2): 1) the proxy data must reflect the precipitation or dry/wet conditions over the monsoon regions; 2) the proxy data span the period between 9.2 and 7.8 ka; and 3) the temporal resolution of proxies must be sufficient to reflect centennial-scale abrupt climate change.

2.4. Definition of GM domain and precipitation

Follow previous studies (Wang and Ding, 2008; Liu et al., 2009a; Wang et al., 2012), the GM domain is defined by the region in which the annual range (AR) of precipitation exceeds 2.0 mm/day, and the local summer precipitation exceeds 55% of annual rainfall. Here AR is defined as May to September (MJJAS) precipitation minus November to March (NDJFM) precipitation in the NH and NDJFM minus MJJAS precipitation in the SH. The GM domain defined by merged CMAP and GPCP data consists of seven regional monsoons: Northern African (NAF), Southern African (SAF), South Asian (SA), East Asian (EA), Australian (AUS), North American (NAM), and South American monsoon (SAM). According to (Liu et al., 2009a) and (Hsu et al., 2012), the NHMP can be measured by the area-averaged mean monsoon precipitation rate in the NH monsoon (NHM) domain during boreal summer (JJA). Similarly, the SHMP can be measured by the area-averaged mean monsoon

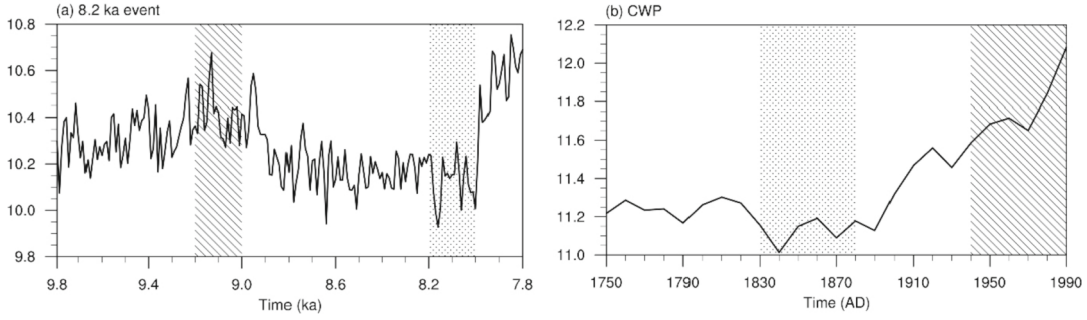

Fig. 2. Time series of decadal mean NH surface temperature derived from the TraCE-AF run. (a) 8.2 ka event and (b) CWP. The hatched represents the selected warm periods, and the stippled represents the selected cold periods.

Table 2
Proxy data used to infer the precipitation changes during the 8.2 ka event.

Monsoon region	Region	Proxy type	Lat	Lon	Change in the 8.2 ka event	Reference
North America	Juxtlahuaca Cave	Seawater $\delta^{18}O$	17°26′N	99°9′W	Drier	Lachniet et al. (2013)
North America	Cueva del Diablo	Stalagmite $\delta^{18}O$	18°11′N	99°55′W	Drier	Bernal et al. (2011)
North America	Pink Panther Cave	Stalagmite $\delta^{18}O$	32°05′N	105°10′W	Drier	Asmerom et al. (2007)
North America	ODP-1002	Titanium and iron concentration	10°43′N	65°10′W	Drier	Haug et al. (2001)
North America	Venado Cave	Stalagmite $\delta^{18}O$	10°6′N	84°8′W	Drier	Lachniet et al. (2004)
North America	Rey Marcos Cave	Stalagmite $\delta^{18}O$	15°24′N	90°18′W	Drier	Winter et al. (2020)
North America	Lake Miragoane	Lake isotopes	18°27′N	73°05′W	Drier	Hodell et al. (1991)
South America	Paixão Cave	Stalagmite $\delta^{18}O$	12°39′S	41°3′W	Wetter	Cheng et al. (2009)
South America	Padre Cave	Stalagmite $\delta^{18}O$	13°13′S	44°3′W	Wetter	Cheng et al. (2009)
South America	Caverna botuverá	Stalagmite $\delta^{18}O$	27°13′S	49°09′W	Wetter	Cruz et al. (2005) Bernal et al. (2016)
South America	Cueva del tigre Perdido Cave	Stalagmite $\delta^{18}O$	5°54′S	77°39′W	Wetter	van Breukelen et al. (2008)
South America	Lapa Grande Cave	Stalagmite $\delta^{18}O$	14°25′S	44°21′W	Wetter	Strikis et al. (2011)
South America	Paraiso Cave	Stalagmite $\delta^{18}O$	4°55′S	55°27′W	Wetter	Wang et al. (2017)
South America	Santiago Cave	Stalagmite $\delta^{18}O$	3°1′S	78°8′W	Wetter	Mosblech et al. (2012)
South America	Jaraguá Cave	Stalagmite $\delta^{18}O$	21°5′S	56°35′W	Wetter	Novello et al. (2019)
uth America	Cueva Del Diamante	Stalagmite $\delta^{18}O$	5°44′S	77°30′W	Wetter	Cheng et al. (2013)
South America	El Condor Cave	Stalagmite $\delta^{18}O$	5°56′S	77°18′W	Wetter	Cheng et al. (2013)
South America	Lake Titicaca	Leaf waxes	16°8′S	69°9′W	Wetter	Fornace et al. (2014)
South Asia	Core 63KA	Laminated sediment	24°37′N	65°58′E	Drier	Staubwasser et al. (2003)
South Asia	Core M5–422	Marine sediment	24°23′N	59°2′E	Drier	Cullen et al. (2000)
South Asia	Qunf Cave	Stalagmite $\delta^{18}O$	17°10′N	54°18′E	Drier	Fleitmann et al. (2003)
South Asia	Hoti Cave	Stalagmite $\delta^{18}O$	23°45′N	57°21′E	Drier	Neff et al. (2001)
South Asia	Mawmluh Cave	Stalagmite $\delta^{18}O$	25°15′N	91°52′E	Drier	Berkelhammer et al. (2013)
North Africa	Core 723A	Marine sediment	18°3′N	57°36′E	Drier	Gupta et al. (2003)
North Africa	ODP-685C	The terrigenous concentration	20°45′N	18°35′W	Drier	deMenocal et al. (2000)
North Africa	Core GeoB4905–4	Seawater $\delta^{18}O$	2°30′N	9°23.04′E	Drier	Weldeab et al. (2005)
North Africa	MD03–2707	Seawater $\delta^{18}O$	2°30′N	9°23′E	Drier	Weldeab et al. (2007)
North Africa	Core RC09–166	Leaf waxes	12°9′N	44°24′E	Drier	Tierney et al. (2017a)
North Africa	Lake Bosumtwi	Leaf waxes	6°30′N	1°25′W	Drier	Shanahan et al. (2015)
North Africa	Core GeoB9508-S	Marine sediment	15°30′N	17°57′W	Drier	Niedermeyer et al. (2010)
North Africa	Core GeoB7920–2	Marine sediment	20°45′N	18°35′W	Drier	Tjallingii et al. (2008)
North Africa	Lake Tana	Lake sediment	12°N	37°15′E	Drier	Costa et al. (2014)
North Africa	GC68	Leaf wax	19°21′N	17°16′W	Drier	Tierney et al. (2017b)
East Asia	Dongge Cave	Stalagmite $\delta^{18}O$	25°17′N	108°5′E	Drier	Wang et al. (2005)
East Asia	Jiuxian Cave	Stalagmite $\delta^{18}O$	33°34′N	109°6′E	Drier	Cai et al. (2010)
East Asia	Heshang Cave	Stalagmite $\delta^{18}O$	30°27′N	110°25′E	Drier	Hu et al. (2008)
East Asia	Lianhua Cave, Shanxi	Stalagmite $\delta^{18}O$	38°10′N	113°43′E	Drier	Dong et al. (2018)
East Asia	Sanbao Cave	Stalagmite $\delta^{18}O$	31°40′N	110°26′E	Drier	Dong et al. (2010)
Australia	Liang Luar Cave	Stalagmite $\delta^{18}O$	8°32′S	120°26′E	Wetter	Ayliffe et al. (2013) Griffiths et al. (2009)
Australia	Gunung Buda	Stalagmite $\delta^{18}O$	4°2′N	114°48′E	Wetter	Partin et al. (2007)
Australia	KNI-51 Cave	Stalagmite $\delta^{18}O$	15°11′S	128°22′E	Wetter	Denniston et al. (2017)
South Africa	Core BJ-03-70GGC	Leaf waxes	3°34′S	119°23′E	Wetter	Tierney et al. (2012)
South Africa	Cold Air Cave	Stalagmite $\delta^{18}O$	24°1′S	29°11′E	Wetter	Holmgren et al. (2003)
South Africa	Anjohibe Cave	Stalagmite $\delta^{18}O$	15°32′S	46°53′E	Wetter	Voarintsoa et al. (2019)
South Africa	Core GeoB9307–3	Marine sediment	18°34′S	37°22.8′E	Wetter	Weldeab et al. (2014)
South Africa	Core GeoB9310–4	Marine sediment	19°12′S	37°2.49′E	Wetter	Weldeab et al. (2014)
South Africa	Lake Tanganyika	Lake sediment	6°6′S	30°E	Drier	Tierney et al. (2008)

precipitation rate in the SH monsoon (SHM) domain during austral summer (DJF). Finally, the GMP is defined by the sum of NHMP and SHMP.

2.5. Moisture budget analysis

We employed a column-integrated moisture budget analysis to reveal the physical process of changes in precipitation over the GM domain during the Holocene abrupt climate change. The moisture equation is written as (Chou et al., 2013)

$$\partial_t\langle q\rangle' + \langle \boldsymbol{V}\bullet\nabla_h q\rangle' + \langle \omega\partial_p q\rangle' = E' - P' \quad (1)$$

where the angle brackets denote the vertical integration from surface to 100 hPa, and the prime means the climatological differences between the two periods. Variable q represents specific humidity, E and P denote the surface evaporation and precipitation, respectively. $\boldsymbol{V}$ and ω denote the horizontal wind and vertical pressure velocity, respectively. $\partial_t\langle q\rangle'$ is the time derivation of vertically integrated moisture, which can be neglected for steady motion. Therefore, the precipitation changes can be expressed as

$$P' = -\langle\overline{\omega}\partial_p q'\rangle - \langle\omega'\partial_p\overline{q}\rangle - \left\langle\overline{V}\bullet\nabla q'\right\rangle - \langle V'\bullet\nabla\overline{q}\rangle + E' + \delta \quad (2)$$

where the overbar represents the climatology in the latter period, the terms $-\langle\overline{\omega}\partial_p q'\rangle$ and $-\langle\omega'\partial_p\overline{q}\rangle$ are the moisture and circulation component of vertical moisture advection, respectively. The terms $-\left\langle\overline{V}\bullet\nabla q'\right\rangle$ and $-\langle V'\bullet\nabla\overline{q}\rangle$ are the moisture and circulation component of horizontal moisture advection, respectively. The residual term includes transient eddies, nonlinear effects, and moisture storage.

3. Results

3.1. Spatiotemporal structure of the GMP during the 8.2 ka event

To identify the 8.2 ka event simulated in the TraCE-AF experiment, we examine the NH averaged surface temperature variation (Fig. 2a). In response to the meltwater injection from 9.0 to 8.0 ka (Fig. 1c), the NH temperature drops rapidly from 9.0 to 8.6 ka and remains in the cold

state until about 8.0 ka. Since the proxy data show a transition from a warm to a cold state across 8.2 ka, we selected the cold period (8.2–8.0 ka) minus the preceding warm period (9.2–9.0 ka) to represent the change during the 8.2 ka event. As a result, the NH temperature decreased by about 0.3 °C during the selected period.

Fig. 3a shows the spatial pattern of the simulated yearly-mean precipitation changes between the cold and the preceding warm period. There is a general decrease of precipitation in the NH while an increase in the SH except over the western Pacific. The largest contrast between the dry NH and wet SH is seen over the tropical Atlantic and eastern Pacific. Significantly drying condition occurs over North America, West Africa, South Asia, and northern East Asia. Over East China, the precipitation anomalies tend to show a 'wet south-dry north' dipolar pattern due to the northward shift of the subtropical rain belt during the boreal summer. In the SH, monsoon precipitation significantly increases, mainly in South America. Since the yearly-mean monsoon precipitation changes are dominated by the local summer precipitation changes, the results shown in Fig. 3 also represent the local summer monsoon precipitation change (Fig. 5c). Note that the paleo archive recorded a robust drying NH monsoon and wetting SH monsoon, which is in good agreement with the model simulated monsoon change (Fig. 3b). On the regional scale, the proxy data indicate a nearly uniform pattern in each monsoon region.

Fig. 4 further compares the evolutions of the precipitation averaged in each monsoon region and each hemispheric monsoon region between the model simulation and the proxy-based precipitation records. Because proxy data are represented by different sets of variables, we standardized the paleoclimate proxy data. We produced the 100-year running mean precipitation time series during the period from 9.2 to 7.8 ka. The NH proxies show a continuous decrease from 9.0 to 8.0 ka (Fig. 4a-e), but there are some differences in NH sub-monsoon regions. In the NAM and NAF monsoon region, there is no recovery of precipitation after 8.0 ka. In the EA, the precipitation change shows a significant inter-centennial fluctuation with a declining trend. The SHM proxy shows a wet condition during 8.8–8.0 ka (Fig. 4f-i). Although there are some uncertainties in the reconstructions, the proxy-based results are in good agreement with the TraCE-AF simulation results, suggesting that the TraCE-AF could capture the spatial and temporal changes of annual mean precipitation during the 9.2 to 7.8 ka.

3.2. Cause of GMP change during the 8.2 ka event

Previous studies suggested that the meltwater injection was a fundamental cause that drove the 8.2 ka event. In addition, the orbital parameters, ice sheet may also play a role. To test this hypothesis, we investigate the contribution of every single forcing on the change in monsoon precipitation during the 8.2 ka event. During 9.2–7.8 ka, the spatial pattern of GMP in the TraCE-MWF experiment resembles closely that in the TraCE-AF simulation, with a pattern correlation coefficient (PCC) = 0.59 (Fig. 5c, d). The NHMP and SHMP in TraCE-MWF is positively correlated with those in TraCE-AF with a correlation coefficient (CC) = 0.92 ($p < 0.1$) and 0.63 ($p < 0.1$), respectively (Fig. 5a, b). It indicates that GMP is primarily forced by meltwater forcing. The spatial pattern of GMP in the TraCE-ORB experiment also exhibits an NH-SH asymmetry, similar to that in TraCE-AF simulation with a PCC = 0.39 (Fig. 5e). It suggests that the orbital parameter might have a moderate contribution to the GMP change. The change in the ice sheet has a minor impact on SHMP (Fig. 5f). In general, the result suggests that changes in GMP are influenced mainly by the meltwater forcing during the 8.2 ka event. The secondary influence of orbital forcing is due to the fact that the examined two periods are one thousand years apart.

3.3. GMP sensitivity and attribution during the 8.2 ka event

To quantitatively assess the sensitivity of monsoon precipitation to the temperature change, we defined the ratio of the change in GMP, NHMP, and SHMP to one-degree census global mean temperature change. In the TraCE-AF experiment, the global mean surface temperature was reduced by 0.12 °C from 9.2–9.0 ka to 8.2–8.0 ka. The NHMP significantly reduced by 1.5% or an equivalent climate sensitivity of 12.4%/°C, while the SHMP slightly increased by 0.5% or 4.2%/°C. In addition, the sensitivity of NHMP and SHMP in the TraCE-MWF experiment reached 23.1%/°C and 4.3%/°C, respectively. The sensitivity of NHMP exceeds the potential moisture-induced sensitivity of about 7%/°C.

Why does the NHMP respond to meltwater forcing more sensitively than the SHMP? We used moisture budget analysis to diagnose the physical processes governing monsoon precipitation changes. Fig. 6a and b compare the results between the NHMP and SHMP. During the 8.2

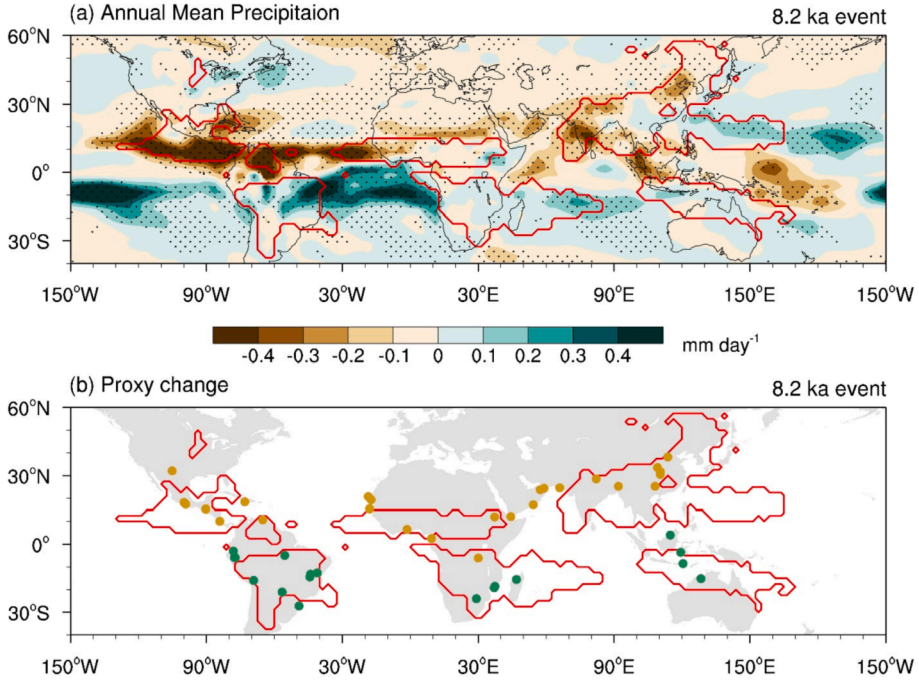

Fig. 3. Comparison between the proxy records and simulated annual mean precipitation during the 8.2 ka event. (a) Difference of the simulated annual mean precipitation between the latter period (8.2–8.0 ka) and preceding period (9.2–9.0 ka) during the 8.2 ka event. (b) Dry (brown) /wet (green) changes inferred from the proxy data (ΔP[8.2–8.0 ka] minus [9.2–9.0 ka]) listed in Table 2. Red lines represent the monsoon regions defined by the merged CMAP and GPCP data. In (a), the dotted region represents the significance above the 95% confidence level via a two-tailed Student's *t*-test. (For interpretation of the references to colour in this figure legend, the reader is referred to the web version of this article.)

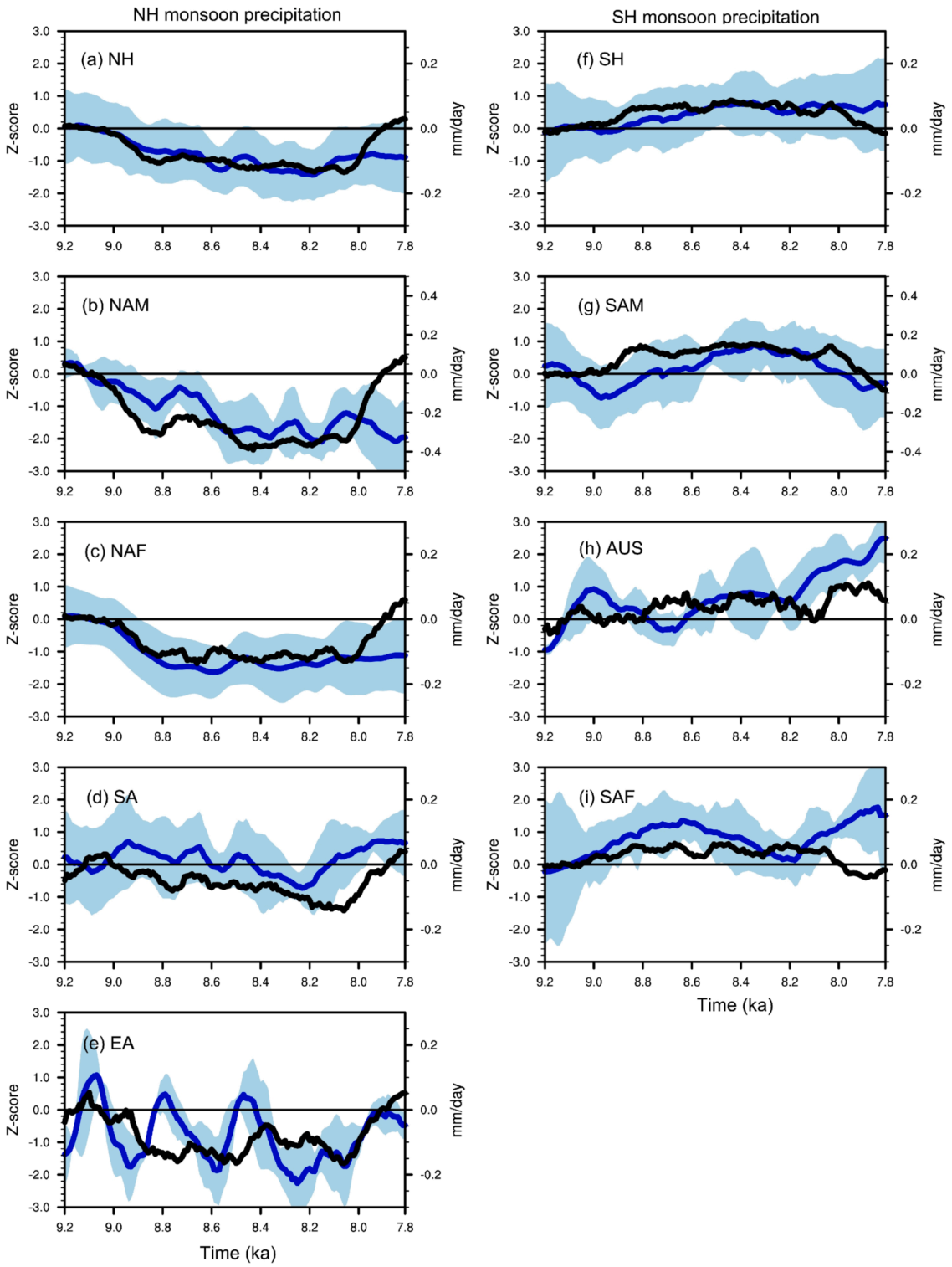

Fig. 4. Comparison of the precipitation evolution inferred from the proxy data (blue) and the simulated annual mean precipitation derived from TraCE-AF (black). (a-e) The proxy data averaged over the NH monsoon regions: (a) NH, (b) NAM, (c) NAF, (d) SA, and (e) EA. (f-i) the proxy records averaged over the SH monsoon regions: (f) SH, (g) SAM, (h) AUS, and (i) SAF. The uncertainty of proxy-based precipitation was measured by 1 standard deviation of the spread of the individual proxy record. A 100-yr running mean has been applied to the time series. *Z*-score denotes the standardized precipitation changes inferred from the proxy data. The simulated annual mean precipitation changes are with reference to the preceding (9.2–9.0 ka) climatology. (For interpretation of the references to colour in this figure legend, the reader is referred to the web version of this article.)

ka event, the circulation change plays an important role in reducing the NHMP, mainly related to the suppressed vertical motion (Fig. 6a). However, the moisture decrease plays a secondary role in the reduced NHMP. By contrast, the moisture increase enhances the SHMP while the circulation change contributes little (Fig. 6b). Thus, the NHMP responds to meltwater forcing more sensitively than the SHMP because the NHMP is affected by the compound circulation and moisture effect. The moisture change mainly influences SHMP change.

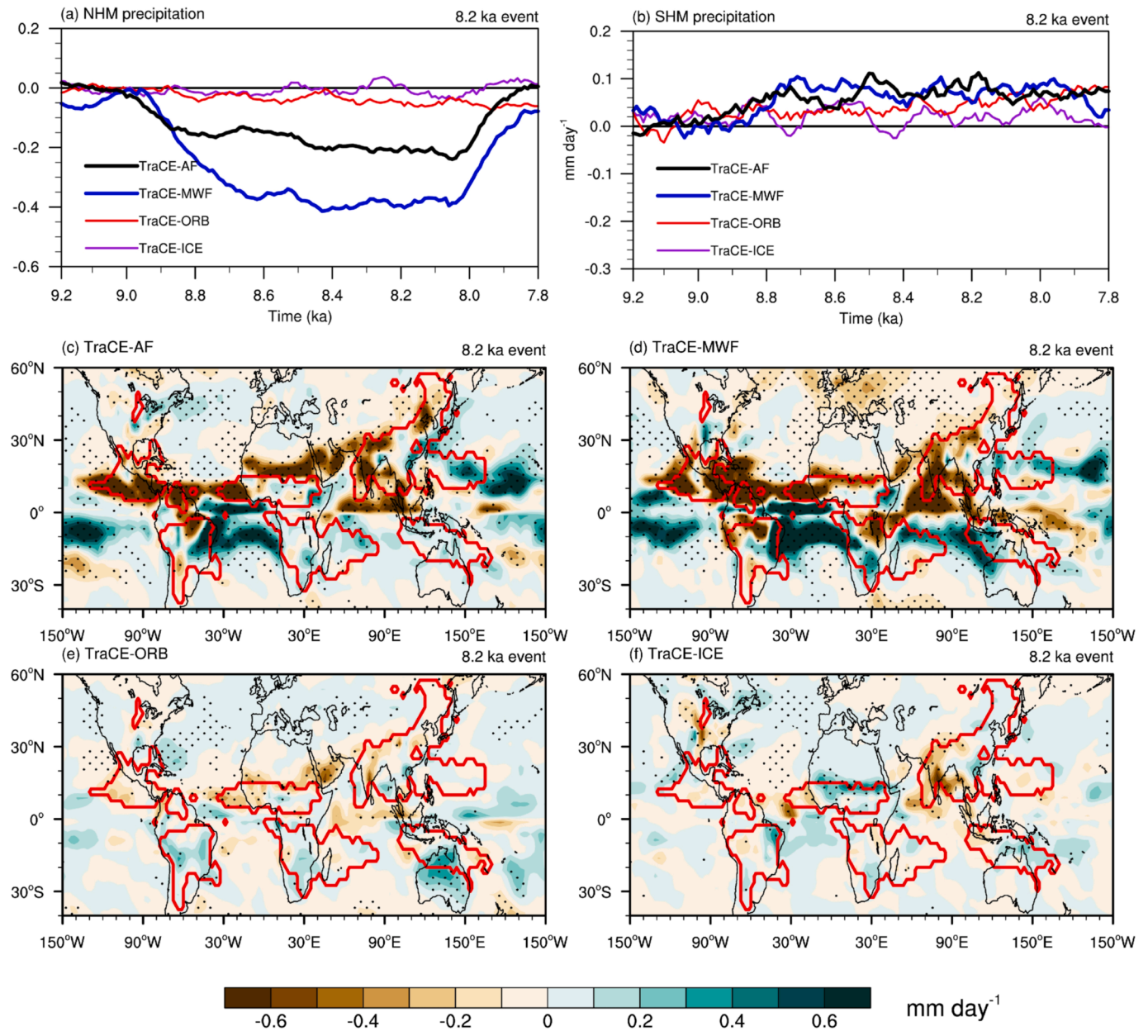

Fig. 5. Spatio-temporal structure of local summer monsoon precipitation rate (mm day^{-1}) during the 8.2 ka event. The upper panels show the time series of summer monsoon precipitation rates averaged over the (a) NHM and (b) SHM regions. Black, blue, red, and purple line indicates the result in the TraCE-AF, TraCE-MWF, TraCE-ORB, and TraCE-ICE, respectively. Boreal summer represents June to August (JJA), and Austral summer means December to February (DJF). The middle and bottom panels show the spatial pattern of local summer precipitation rate changes derived from TraCE all forcing and four single-forcing experiments: (c) TraCE-AF, (d) TraCE-MWF, (e)TraCE-ORB, and (f) TraCE-ICE. Changes are measured by the latter period (8.2–8.0 ka) relative to the preceding period (9.2–9.0 ka). The dots denote regions in which the changes are significant at the 95% confidence level via a two-tailed Student's *t*-test. The red line represents the GM domain. (For interpretation of the references to colour in this figure legend, the reader is referred to the web version of this article.)

4. Discussions

4.1. Common processes that drive the GMP change

What are the fundamental causes of the circulation and moisture change? Fig. 6c-h present spatial distribution of the changes in the surface temperature, sea-level pressure (SLP), and specific humidity and winds at 850 hPa. The increase in meltwater discharge reduced the surface seawater salinity in the North Atlantic, weakening the AMOC (Ba et al., 2014). The weakened AMOC further decreased the northward heat transport between the two hemispheres, leading to an overall cooling of the North Atlantic. The North Atlantic cooling is further spread to other parts of the NH, especially in high-latitude regions (Fig. 6c, d). The spreading processes of North Atlantic cooling have been demonstrated by numerical experiments (Yang et al., 2020). Such interhemispheric temperature changes cause a robust NH-SH meridional gradient in the SLP. During boreal summer, the increased NH SLP weakens the climatological northward cross-equatorial flow (Fig. 6e) and transport of moist static energy, decreasing moisture convergence and NHMP. During austral summer (DJF), the enhanced NH SLP enhances the southward cross-equatorial transport of the boundary layer's moist static energy (Fig. 6f), increasing the moisture convergence and SHMP. Thus, the NH cooling and SH warming favor a "drier NH monsoon and wetter SH monsoon" (Fig. 5d). Fig. 7a shows that the NHMP decrease is highly related to the interhemispheric temperature changes in the meltwater experiments. It suggests that the meltwater-

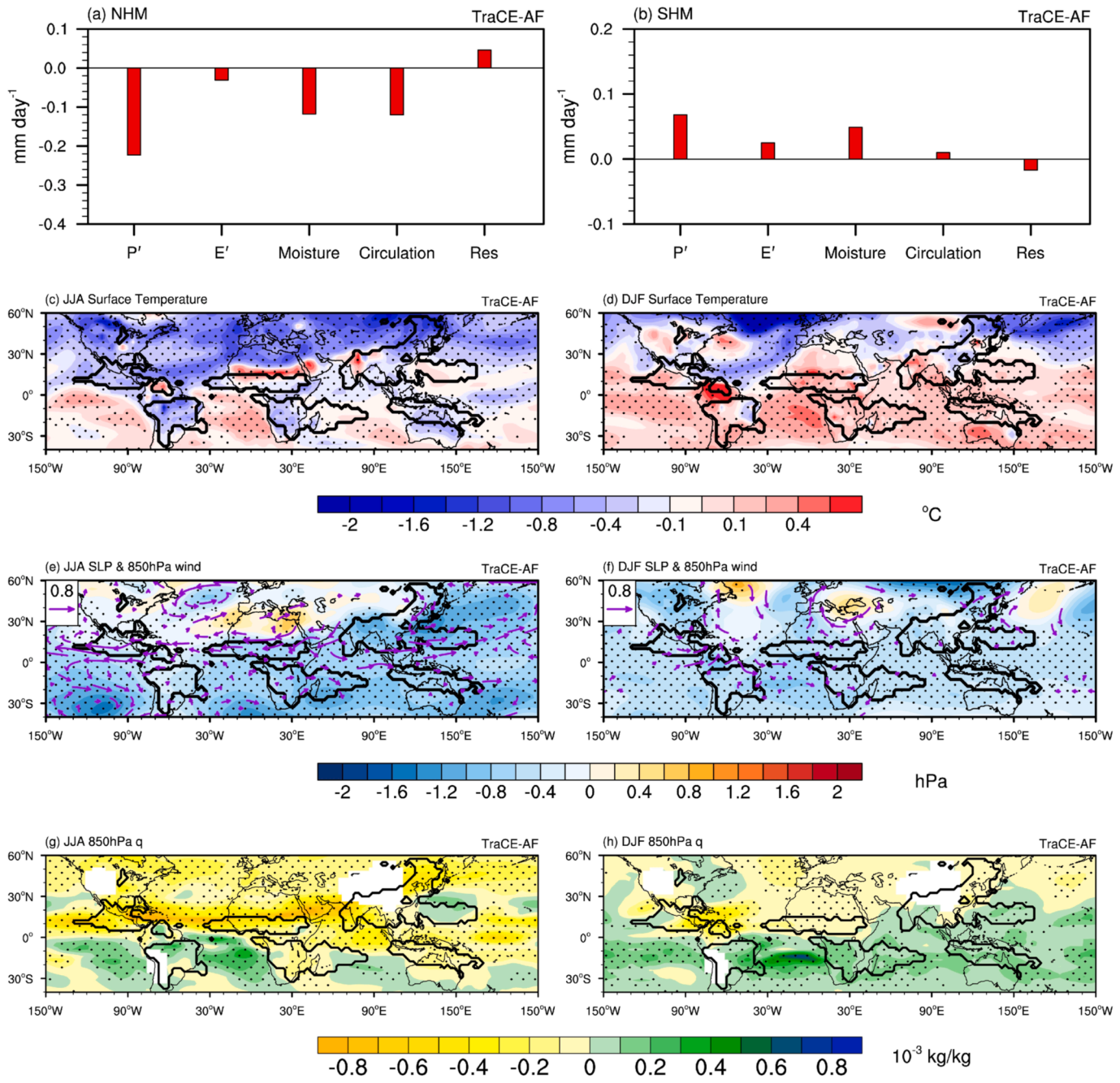

Fig. 6. Atmosphere moisture and circulation change during the 8.2 ka event derived from the TraCE-AF experiment. (a, b) Moisture budget decomposition of local summer precipitation (mm day^{-1}) changes. (c, d) Surface temperature (°C) changes, (e, f) Sea level pressure (shadings, hPa) and 850 hPa wind (vectors, m s^{-1}) changes, and (g, h) 850 hPa specific humidity (kg kg^{-1}) changes in JJA mean. Only the regions where significant above the 95% confidence level via a two-tailed Student's *t*-test are dotted.

induced hemispheric thermal contrast is one of the fundamental causes of the GMP change.

It is conceivable that the land-ocean thermal contrast change induced by the meltwater forcing may also contribute to decreasing NHMP as the relative cooling over land may lead to weakening the climatological land low-pressure system (Fig. 6e) that may prohibit the low-level moisture flows from converging into monsoon regions (Wang et al., 2020). To test the hypothesis, we have examined the relationship between the changes of NHMP and the land-ocean thermal contrast during the 8.2 ka event. As shown in Fig. 7c, the changes of NHMP are significantly correlated with the land-ocean thermal contrast that measure by the land minus ocean surface temperature. The result shows that reduced land-ocean thermal contrast reproduced weaker NHMP. The North American summer monsoon precipitation changes are highly correlated to the temperature gradients between the equatorial eastern Pacific and the tropical Atlantic (Wang et al., 2020). It is confirmed by the relationship shown in Fig. 7e.

We now turn our attention to the GMP change in the CWP under the increasing GHG forcing to contrast the changes arising from the meltwater-induced cooling. What are the characteristics of GMP under the CWP? During the CWP (Fig. 8), the NHMP change featured an east-west asymmetry between the enhanced Asian-African monsoon and reduced North American monsoon rainfall, which is similar to the future change of NHMP (Lee and Wang, 2014; Wang et al., 2020). In the TraCE-AF experiment, the GMP averaged precipitation rate increases by 1% or 2.0%/°C, which is close to the previous results (Chai et al., 2018). The

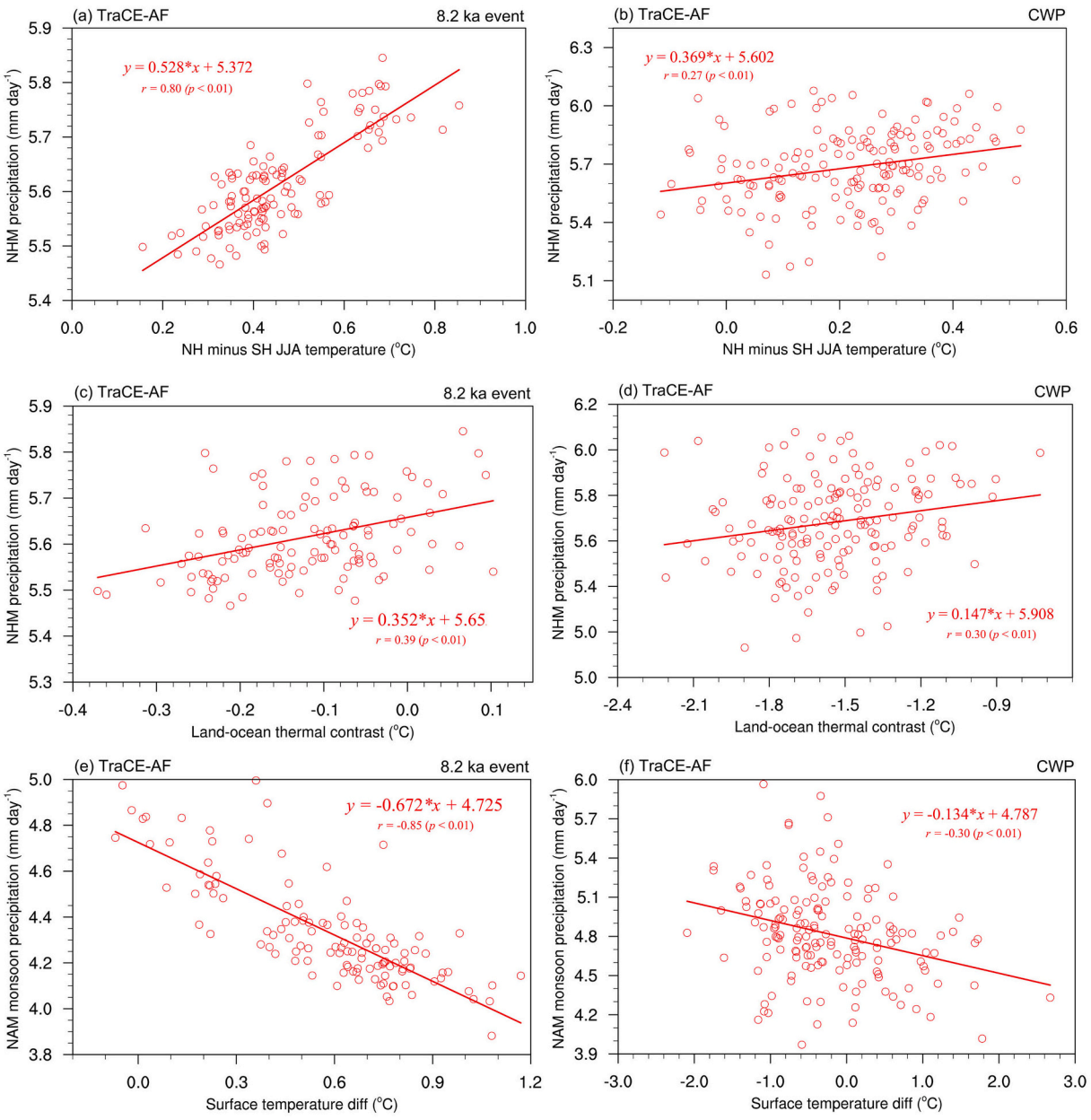

Fig. 7. Relationships between the monsoon precipitation and lower boundary forcing. (a, b) the NHMP as a function of the hemispheric thermal contrast (T2m for 0°-60°N,0°-360°E minus T2m for 40°-0°,0°-360°E). (c, d) NHMP as a function of the surface temperature difference over the land region (0°-60°N, 0°-360°E) and adjacent ocean region (0°-60°N, 0°-360°E). (e, f) the JJA mean NAM (North American) monsoon precipitation as a function of the surface temperature difference between equatorial eastern Pacific (5°S-5°N, 120°-80°W) and the tropical Atlantic (10°-20°N, 60°-15°W).

NHMP and SHMP increases by 1.8%/°C and 2.2%/°C, respectively. Comparing with the sensitivity during the 8.2 ka event and CWP, we found that GMP response to meltwater and GHG forcing is different. Why does this happen? In the CWP, the moisture effect plays a vital role in enhancing the NHMP and SHMP (Fig. 9a, b), mainly related to the specific humidity increase (Fig. 9e, f). The circulation effect tends to reduce the precipitation, especially the SHMP. The reason is that the GHG-induced vertically differential radiative forcing increases atmospheric static stability. Based on the Clausius-Clapeyron relation, the moisture content in a saturated air column increases with the air temperature at a rate of ~7%/°C (Trenberth, 1998; Allen and Ingram, 2002), while the results here show a moderate increase of about 2.0%/°C in GMP due to the offset between the moisture and circulation effect. In contrast, the sensitivity of the GMP to temperature in the 8.2 ka event exceeds 7%/°C due to the circulation response reinforces the moisture effect.

Although the GMP changes in the CWP and the 8.2 ka event differ, they share common drivers. The external forcing-induced horizontally differential temperature changes determine the corresponding circulation change, and the latter is responsible for the spatial structure of the precipitation change. The circulation changes are associated with interhemispheric thermal contrast, land-ocean thermal contrast, and tropical SST pattern. To illustrate this argument, we first examined the change in interhemispheric thermal contrast under the CWP. The non-uniform warming induced by the GHGs' radiative forcing leads to "NH warmer than SH" (Fig. 9c, d). The anomalous temperature gradient enhanced the anomalous cross-equatorial pressure gradients that drive low-level cross-equatorial flows from SH to NH, increasing the NHMP (Fig. 7b). Moreover, in the CWP, the horizontally differential warming results in a "land warmer than ocean" pattern. As shown in Fig. 7d, a

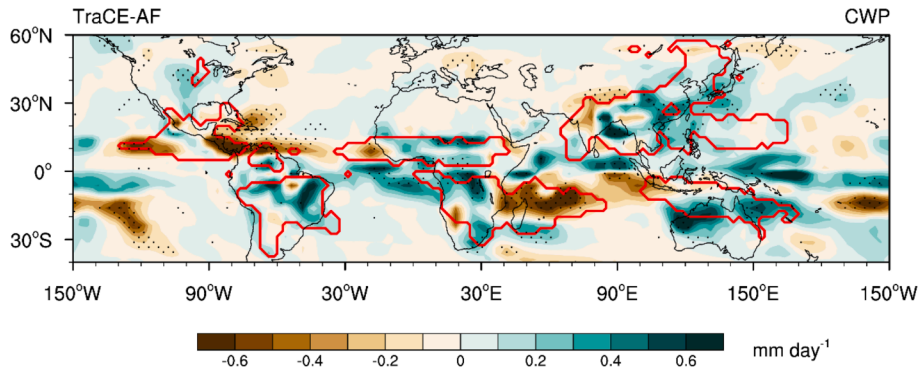

Fig. 8. Local summer precipitation changes during the CWP derived from TraCE-AF. Only the regions where the significance is above the 95% confidence level via a two-tailed Student's *t-test* are dotted.

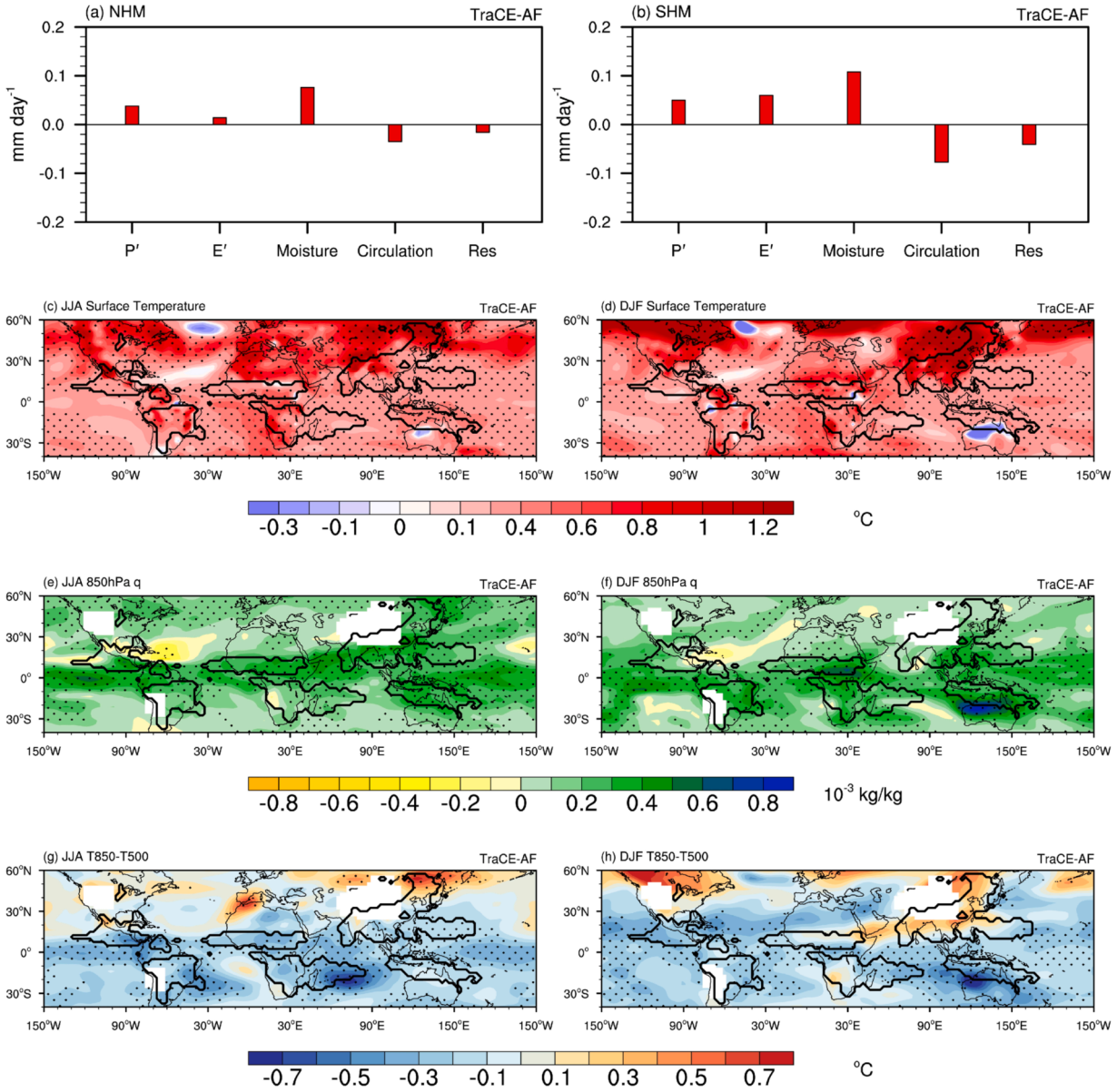

Fig. 9. Atmosphere moisture and circulation change during the CWP derived from the TraCE-AF experiment. (a, b) Moisture budget decomposition of local summer precipitation changes. (c) Surface temperature (shadings, °C) changes. (e) 850 hPa specific humidity (shadings, kg kg^{-1}) changes. (g) Atmospheric static stability changes (shadings, °C) in JJA mean. (c, e, and g) same as (d, f, and h), but for the result in DJF mean. Only the significant regions above the 95% confidence level via a two-tailed Student's *t-test* are dotted.

larger change in the land-ocean thermal contrast generates stronger NHMP. In addition, the North American summer monsoon precipitation changes are significantly correlated to the temperature gradients between the equatorial eastern Pacific and the tropical Atlantic (Fig. 7f). In summary, although there are apparent differences in the spatial distribution and sensitivity of GMP between the 8.2 ka event and CWP, there are common processes that drive GMP change in the past and the present day.

4.2. Perspective

This study takes an important step toward improving our understanding of GMP response to the 8.2 ka event. By comparing the change of GMP in the 8.2 ka event, CWP, and future (Wang et al., 2020), an important suggestion is that the hemispheric thermal contrast, land-ocean thermal contrast, and tropical SST gradients are common drivers of the NHMP changes in the past, present, and future.

Although the meltwater forcing plays a crucial role in the 8.2 ka event, solar activity and volcanic eruption may indeed have contributed to the 8.2 ka event. Firstly, the 8.2 ka cooling events may have been driven by increases in North Atlantic Arctic drift ice induced by a quasiperiodic decline in sunspot activity (Wang et al., 2005). Diluted sea waters would have slowed the AMOC, leading to the cooling of the NH (Bond, 2001). Secondly, there were three major volcanic eruptions during the 8288–8178 BP, which could have exacerbated the climate impact caused by the meltwater discharge (Cole-Dai et al., 2021). Systematic examination and modeling studies are needed to investigate further the role of solar and volcanic activity in the 8.2 ka event.

In the meltwater experiments, the other forcings (ice sheet, orbital, and GHGs) were fixed at the 19 ka conditions. This design might substantially affect the mean climate around 8.2 ka. Therefore, a considerably colder climate mean-state is expected. This caveat might affect the GM response to the meltwater response in the meltwater experiment. Besides, the simulation was conducted with a single climate model. The model's physical parameterization may cause uncertainties. The multi-model simulation results are needed to verify the quantitative conclusions presented here.

5. Conclusion

Based on a large set of hydroclimate archives during the 8.2 ka event, we find that the GMP simulated by TraCE-AF experiments features a robust NH-SH asymmetry, which is consistent with the proxy data. By comparing the TraCE-AF and single-forcing experiments, we illustrate the GMP change in the 8.2 ka event mainly attributed to the meltwater injection with a moderate contribution from the orbital forcing. During the 8.2 ka event, the NHMP responds to meltwater forcing more sensitively than the SHMP. The moisture budget analysis suggests that weakened circulation (upward motion) plays a dominant role in reducing the NHMP. Furthermore, the reduced specific humidity reinforces the precipitation decrease. On the other hand, the moisture increase plays an main role in enhancing the SHMP. The sensitivity of NHMP in the CWP is significantly lower than the 8.2 ka event. In the CWP, the increased moisture tends to enhance precipitation, but the vertically differential radiative forcing-induced atmospheric static stability increase, reducing the dynamic (moisture convergence) effect. Thus, the two thermodynamic effects (increased moisture content and static stability) partially offset each other.

The meltwater and greenhouse gas forcings induce differing global temperature change patterns and circulation changes. However, the GMP changes are governed by common root causes, namely, through the external forcing-induced NH-SH thermal contrast, land-ocean thermal contrast, and the tropical SST gradients. The moisture change plays a crucial role in altering precipitation amount but not spatial distribution. The external forcing-induced warming (cooling) pattern drives the circulation changes (dynamic effects), determining the spatial structure of the monsoon rainfall changes in the past and the present.

Declaration of Competing Interest

The authors declare that they have no known competing financial interests or personal relationships that could have appeared to influence the work reported in this paper.

Acknowledgments

We thank the CMAP and GPCP for the observation data. This work was jointly supported by the National Natural Science Foundation of China (Grant Nos. 42130604, 42105044, 41971108, 42111530182, and 91437218) and the Priority Academic Program Development of Jiangsu Higher Education Institutions (Grant No. 164320H116).

References

Acosta Navarro, J.C., Ekman, A.M., Pausata, F.S., Lewinschal, A., Varma, V., Seland, Ø., Gauss, M., Iversen, T., Kirkevåg, A., Riipinen, I., Hansson, H.C., 2017. Future response of temperature and precipitation to reduced aerosol emissions as compared with increased greenhouse gas concentrations. J. Clim. 30, 939–954. https://doi.org/10.1175/JCLI-D-16-0466.1.

Adler, R.F., Sapiano, M.R.P., Huffman, G.J., Wang, J.-J., Gu, G., Bolvin, D., Chiu, L., Schneider, U., Becker, A., Nelkin, E., Xie, P., Ferraro, R., Shin, D.-B., 2018. The Global Precipitation Climatology Project (GPCP) monthly analysis (new version 2.3) and a review of 2017 global precipitation. Atomosphere 9, 138. https://doi.org/10.3390/atmos9040138.

Allen, M.R., Ingram, W.J., 2002. Constraints on future changes in climate and the hydrologic cycle. Nature 419, 228–232. https://doi.org/10.1038/nature01092.

Alley, R., Agustsdottir, A., 2005. The 8k event: cause and consequences of a major Holocene abrupt climate change. Quat. Sci. Rev. 24, 1123–1149. https://doi.org/10.1016/j.quascirev.2004.12.004.

Alley, R.B., Mayewski, P.A., Sowers, T., Stuiver, M., Taylor, K.C., Clark, P.U., 1997. Holocene climatic instability: A prominent, widespread event 8200 yr ago. Geology 25. https://doi.org/10.1130/0091-7613(1997)025<0483:HCIAPW>2.3.CO;2, 483-468.

Alley, R.B., Marotzke, J., Nordhaus, W.D., Overpeck, J.T., Peteet, D.M., Pielke, R.A., 2003. Abrupt climate change. Science 299, 2005–2010. https://doi.org/10.1126/science.1081056.

An, Z., Wu, G., Li, J., Sun, Y., Liu, Y., Zhou, W., Cai, Y., Duan, A., Li, L., Mao, J., Cheng, H., Shi, Z., Tan, L., Yan, H., Ao, H., Chang, H., Feng, J., 2015. Global monsoon dynamics and climate change. Annu. Rev. Earth Planet. Sci. 43, 29–77. https://doi.org/10.1146/annurev-earth-060313-054623.

Andrews, J.T., Smith, L.M., Preston, R., Cooper, T., Jennings, A.E., 1997. Spatial and temporal patterns of iceberg rafting (IRD) along the East Greenland margin, ca. 68°N, over the last 14 cal.ka. J. Quat. Sci. 12, 1–13. https://doi.org/10.1002/(SICI)1099-1417(199701/02)12:1<1::AID-JQS288>3.0.CO;2-T.

Asmerom, Y., Polyak, V., Burns, S., Rassmussen, J., 2007. Solar forcing of Holocene climate: New insights from a speleothem record, southwestern United States. Geology 35, 1–4. https://doi.org/10.1130/G22865A.1.

Ayliffe, L.K., Gagan, M.K., Zhao, J., Drysdale, R.N., Hellstrom, J.C., Hantoro, W.S., Griffiths, M.L., Scott-Gagan, H., Pierre, E.S., Cowley, J.A., Suwargadi, B.W., 2013. Rapid interhemispheric climate links via the Australasian monsoon during the last deglaciation. Nat. Commun. 4, 2908. https://doi.org/10.1038/ncomms3908.

Ba, J., Keenlyside, N.S., Latif, M., Park, W., Ding, H., Lohmann, K., Mignot, J., Menary, M., Otterå, O.H., Wouters, B., Melia, D.S., Oka, A., Bellucci, A., Volodin, E., 2014. A multi-model comparison of Atlantic multidecadal variability. Clim. Dyn. 43, 2333–2348. https://doi.org/10.1007/s00382-014-2056-1.

Barber, D., Dyke, A., Hillaire-Marcel, C., Jennings, A.E., Andrews, J.T., Kerwin, M.W., Bilodeau, G., McNeely, R., Southon, J., Morehead, M.D., Gagnon, J.-M., 1999. Forcing of the cold event of 8,200 years ago by catastrophic drainage of Laurentide lakes. Nature 400, 344–348. https://doi.org/10.1038/22504.

Bauer, E., Ganopolski, A., 2004. Simulation of the cold climate event 8200 years ago by meltwater outburst from Lake Agassiz. Paleoceanography 19, PA3014. https://doi.org/10.1029/2004PA001030.

Berger, A.L., 1978. Long-term variations of daily insolation and Quaternary climatic changes. J. Atmos. Sci. 35, 2362–2367 (doi:10.1175/1520- 0469(1978)035<2362:LTVODI>2.0.CO;2).

Berkelhammer, M., Sinha, A., Stott, L., Cheng, H., Pausata, F.S.R., Yoshimura, K., 2013. An abrupt shift in the Indian monsoon 4000 years ago. In: Giosan, L., Fuller, D.Q., Nicoll, K., Flad, R.K., Clift, P.D. (Eds.), Geophysical Monograph Series. American Geophysical Union, Washington, D. C., pp. 75–88. https://doi.org/10.1029/2012GM001207

Bernal, J.P., Lachniet, M., McCulloch, M., Mortimer, G., Morales, P., Cienfuegos, E., 2011. A speleothem record of Holocene climate variability from southwestern Mexico. J. Quat. Res. 75, 104–113. https://doi.org/10.1016/j.yqres.2010.09.002.

Bernal, J.P., Cruz, F.W., Stríkis, N.M., Wang, X., Deininger, M., Catunda, M.C.A., Ortega-Obregón, C., Cheng, H., Edwards, R.L., Auler, A.S., 2016. High-resolution Holocene South American monsoon history recorded by a speleothem from Botuverá Cave,

Brazil. Earth Planet. Sci. Lett. 450, 186–196. https://doi.org/10.1016/j.epsl.2016.06.008.
Bond, G., 1997. A pervasive millennial-scale cycle in North Atlantic holocene and glacial climates. Science 278, 1257–1266. https://doi.org/10.1126/science.278.5341.1257.
Bond, G., 2001. Persistent solar influence on North Atlantic climate during the holocene. Science 294, 2130–2136. https://doi.org/10.1126/science.1065680.
Cai, Y., Tan, L., Cheng, H., An, Z., Edwards, R.L., Kelly, M.J., Kong, X., Wang, X., 2010. The variation of summer monsoon precipitation in central China since the last deglaciation. Earth Planet. Sci. Lett. 291, 21–31. https://doi.org/10.1016/j.epsl.2009.12.039.
Chai, J., Liu, F., Liu, J., Shen, X., 2018. Enhanced global monsoon in present warm period due to natural and anthropogenic forcings. Atmosphere 9, 136. https://doi.org/10.3390/atmos9040136.
Cheng, H., Fleitmann, D., Edwards, R.L., Wang, X., Cruz, F.W., Auler, A.S., Mangini, A., Wang, Y., Kong, X., Burns, S.J., Matter, A., 2009. Timing and structure of the 8.2 kyr B.P. event inferred from $\delta^{18}O$ records of stalagmites from China, Oman, and Brazil. Geology 37, 1007–1010. https://doi.org/10.1130/G30126A.1.
Cheng, H., Sinha, A., Cruz, F.W., Wang, X., Edwards, R.L., d'Horta, F.M., Ribas, C.C., Vuille, M., Stott, L.D., Auler, A.S., 2013. Climate change patterns in Amazonia and biodiversity. Nat. Commun. 4, 1411. https://doi.org/10.1038/ncomms2415.
Cheng, J., Ma, W., Liu, Z., Wu, H., 2019. Varying sensitivity of East Asia summer monsoon circulation to temperature change since last glacial maximum. Geophys. Res. Lett. 46, 9103–9109. https://doi.org/10.1029/2019GL083405.
Chou, C., Chiang, J.C.H., Lan, C.-W., Chung, C.-H., Liao, Y.-C., Lee, C.-J., 2013. Increase in the range between wet and dry season precipitation. Nat. Geosci. 6, 263–267. https://doi.org/10.1038/ngeo1744.
Clark, P.U., Shakun, J.D., Baker, P.A., Bartlein, P.J., Brewer, S., Brook, E., Carlson, A.E., Cheng, H., Kaufman, D.S., Liu, Z., Marchitto, T.M., Mix, A.C., Morrill, C., Otto-Bliesner, B.L., Pahnke, K., Russell, J.M., Whitlock, C., Adkins, J.F., Blois, J.L., Clark, J., Colman, S.M., Curry, W.B., Flower, B.P., He, F., Johnson, T.C., Lynch-Stieglitz, J., Markgraf, V., McManus, J., Mitrovica, J.X., Moreno, P.I., Williams, J.W., 2012. Global climate evolution during the last deglaciation. Proc. Natl. Acad. Sci. U. S. A. 109, E1134–E1142. https://doi.org/10.1073/pnas.1116619109.
Clarke, G.K.C., Leverington, D.W., Teller, J.T., Dyke, A.S., 2004. Paleohydraulics of the last outburst flood from glacial Lake Agassiz and the 8200BP cold event. Quat. Sci. Rev. 23, 389–407. https://doi.org/10.1016/j.quascirev.2003.06.004.
Cole-Dai, J., Ferris, D.G., Kennedy, J.A., Sigl, M., McConnell, J.R., Fudge, T.J., Geng, F., Maselli, O.J., Taylor, K.C., Souney, J.M., 2021. Comprehensive record of volcanic eruptions in the Holocene (11,000 years) from the WAIS divide, Antarctica Ice core. J. Geophys. Res.-Atmos. 126 https://doi.org/10.1029/2020JD032855 e2020JD032855.
Costa, K., Russell, J., Konecky, B., Lamb, H., 2014. Isotopic reconstruction of the African humid period and Congo air boundary migration at Lake Tana. Ethiopia. Quat. Sci. Rev. 83, 58–67. https://doi.org/10.1016/j.quascirev.2013.10.031.
Cruz, F.W., Burns, S.J., Karmann, I., Sharp, W.D., Vuille, M., Cardoso, A.O., Ferrari, J.A., Silva Dias, P.L., Viana, O., 2005. Insolation-driven changes in atmospheric circulation over the past 116,000 years in subtropical Brazil. Nature 434, 63–66. https://doi.org/10.1038/nature03365.
Cullen, H.M., Hemming, G., Brown, F.H., Guilderson, T., Sirocko, F., 2000. Climate change and the collapse of the Akkadian empire: Evidence from the deep sea. Geology 28, 379–382. https://doi.org/10.1130/0091-7613(2000)028<0379:CCATCO>2.3.CO;2.
D'Agostino, R., Bader, J., Bordoni, S., Ferreira, D., Jungclaus, J., 2019. Northern hemisphere monsoon response to mid-holocene orbital forcing and greenhouse gas-induced global warming. Geophys. Res. Lett. 46, 1591–1601. https://doi.org/10.1029/2018GL081589.
deMenocal, P., Ortiz, J., Guilderson, T., Sarnthein, M., 2000. Coherent high- and low-latitude climate variability during the Holocene warm period. Science 288, 2198–2202. https://doi.org/10.1126/science.288.5474.2198.
Denniston, R.F., Asmerom, Y., Polyak, V.J., Wanamaker, A.D., Ummenhofer, C.C., Humphreys, W.F., Cugley, J., Woods, D., Lucker, S., 2017. Decoupling of monsoon activity across the northern and southern Indo-Pacific during the Late Glacial. Quat. Sci. Rev. 176, 101–105. https://doi.org/10.1016/j.quascirev.2017.09.014.
Dixit, Y., Hodell, D.A., Sinha, R., Petrie, C.A., 2014. Abrupt weakening of the Indian summer monsoon at 8.2 kyr BP. Earth Planet. Sci. Lett. 391, 16–23. https://doi.org/10.1016/j.epsl.2014.01.026.
Dong, J., Wang, Y., Cheng, H., Hardt, B., Edwards, R.L., Kong, X., Wu, J., Chen, S., Liu, D., Jiang, X., Zhao, K., 2010. A high-resolution stalagmite record of the Holocene East Asian monsoon from Mt Shennongjia, central China. The Holocene 20, 257–264. https://doi.org/10.1177/0959683609350393.
Dong, J., Shen, C.-C., Kong, X., Wu, C.-C., Hu, H.-M., Ren, H., Wang, Y., 2018. Rapid retreat of the East Asian summer monsoon in the middle Holocene and a millennial weak monsoon interval at 9 ka in northern China. J. Asian Earth Sci. 151, 31–39. https://doi.org/10.1016/j.jseaes.2017.10.016.
Finkenbinder, M.S., Abbott, M.B., Steinman, B.A., 2016. Holocene climate change in Newfoundland reconstructed using oxygen isotope analysis of lake sediment cores. Glob. Planet. Chang. 143, 251–261. https://doi.org/10.1016/j.gloplacha.2016.06.014.
Fleitmann, D., Burns, S.J., Mudelsee, M., Neff, U., Kramers, J., Mangini, A., Matter, A., 2003. Holocene forcing of the Indian monsoon recorded in a stalagmite from Southern Oman. Science 300, 1737–1739. https://doi.org/10.1126/science.1083130.
Fornace, K.L., Hughen, K.A., Shanahan, T.M., Fritz, S.C., Baker, P.A., Sylva, S.P., 2014. A 60,000-year record of hydrologic variability in the Central Andes from the hydrogen isotopic composition of leaf waxes in Lake Titicaca sediments. Earth Planet. Sci. Lett. 408, 263–271. https://doi.org/10.1016/j.epsl.2014.10.024.
Griffiths, M.L., Drysdale, R.N., Gagan, M.K., Zhao, J.-X., Ayliffe, L.K., Hellstrom, J.C., Hantoro, W.S., Frisia, S., Feng, Y.X., Cartwright, I., St Pierre, E., Fischer, M.J., Suwargadi, B.W., 2009. Increasing Australian–Indonesian monsoon rainfall linked to early Holocene sea-level rise. Nat. Geosci. 2, 636–639. https://doi.org/10.1038/ngeo605.
Gupta, A.K., Anderson, D.M., Overpeck, J.T., 2003. Abrupt changes in the Asian southwest monsoon during the Holocene and their links to the North Atlantic Ocean. Nature 421, 354–357. https://doi.org/10.1038/nature01340.
Haug, G.H., Hughen, K.A., Sigman, D.M., Peterson, L.C., Röhl, U., 2001. Southward migration of the intertropical convergence zone through the holocene. Science 293, 1304–1308. https://doi.org/10.1126/science.1059725.
He, F., 2011. Simulating Transient Climate Evolution of the Last Deglaciation with CCSM3. University of Wisconsin–Madison (185 pp).
He, F., Shakun, J.D., Clark, P.U., Carlson, A.E., Liu, Z., Otto-Bliesner, B.L., Kutzbach, J.E., 2013. Northern Hemisphere forcing of Southern Hemisphere climate during the last deglaciation. Nature 494, 81–85. https://doi.org/10.1038/nature11822.
Hodell, D.A., Curtis, J.H., Jones, G.A., Higuera-Gundy, A., Brenner, M., Binford, M.W., Dorsey, K.T., 1991. Reconstruction of Caribbean climate change over the past 10,500 years. Nature 352, 790–793. https://doi.org/10.1038/352790a0.
Holmes, J., Lowe, J., Wolff, E., Srokosz, M., 2011. Rapid climate change: lessons from the recent geological past. Glob. Planet. Chang. 79, 157–162. https://doi.org/10.1016/j.gloplacha.2010.10.005.
Holmgren, K., Lee-Thorp, J.A., Cooper, G.R.J., Lundblad, K., Partridge, T.C., Scott, L., Sithaldeen, R., Siep Talma, A., Tyson, P.D., 2003. Persistent millennial-scale climatic variability over the past 25,000 years in Southern Africa. Quat. Sci. Rev. 22, 2311–2326. https://doi.org/10.1016/S0277-3791(03)00204-X.
Hsu, P., Li, T., Luo, J.-J., Murakami, H., Kitoh, A., Zhao, M., 2012. Increase of global monsoon area and precipitation under global warming: A robust signal? Geophys. Res. Lett. 39, L06701. https://doi.org/10.1029/2012GL051037.
Hu, C., Henderson, G.M., Huang, J., Xie, S., Sun, Y., Johnson, K.R., 2008. Quantification of Holocene Asian monsoon rainfall from spatially separated cave records. Earth Planet. Sci. Lett. 266, 221–232. https://doi.org/10.1016/j.epsl.2007.10.015.
Joos, F., Spahni, R., 2008. Rates of change in natural and anthropogenic radiative forcing over the past 20,000 years. Proc. Natl. Acad. Sci. U. S. A. 105, 1425–1430. https://doi.org/10.1073/pnas.0707386105.
Lachniet, M.S., Asmerom, Y., Burns, S.J., Patterson, W.P., Polyak, V.J., Seltzer, G.O., 2004. Tropical response to the 8200 yr B.P. cold event? Speleothem isotopes indicate a weakened early Holocene monsoon in Costa Rica. Geology 32, 957–960. https://doi.org/10.1130/G20797.1.
Lachniet, M.S., Asmerom, Y., Bernal, J.P., Polyak, V.J., Vazquez-Selem, L., 2013. Orbital pacing and ocean circulation-induced collapses of the Mesoamerican monsoon over the past 22,000 y. Proc. Natl. Acad. Sci. U. S. A. 110, 9255–9260. https://doi.org/10.1073/pnas.1222804110.
Lee, J.-Y., Wang, B., 2014. Future change of global monsoon in the CMIP5. Clim. Dyn. 42, 101–119. https://doi.org/10.1007/s00382-012-1564-0.
Liu, J., Wang, B., Ding, Q., Kuang, X., Soon, W., Zorita, E., 2009a. Centennial Variations of the Global Monsoon Precipitation in the Last Millennium: Results from ECHO-G Model. J. Clim. 22, 2356–2371. https://doi.org/10.1175/2008JCLI2353.1.
Liu, Z., Otto-Bliesner, B.L., He, F., Brady, E.C., Tomas, R., Clark, P.U., Carlson, A.E., Lynch-Stieglitz, J., Curry, W., Brook, E., Erickson, D., Jacob, R., Kutzbach, J., Cheng, J., 2009b. Transient simulation of last deglaciation with a new mechanism for bolling-allerod warming. Science 325, 310–314. https://doi.org/10.1126/science.1171041.
Liu, J., Wang, B., Yim, S.-Y., Lee, J.-Y., Jhun, J.-G., Ha, K.-J., 2012. What drives the global summer monsoon over the past millennium? Clim. Dyn. 39, 1063–1072. https://doi.org/10.1007/s00382-012-1360-x.
Liu, W., Xie, S.-P., Liu, Z., Zhu, J., 2017. Overlooked possibility of a collapsed Atlantic Meridional Overturning Circulation in warming climate. Sci. Adv. 3, e1601666 https://doi.org/10.1126/sciadv.1601666.
Matero, I.S.O., Gregoire, L.J., Ivanovic, R.F., Tindall, J.C., Haywood, A.M., 2017. The 8.2 ka cooling event caused by Laurentide ice saddle collapse. Earth Planet Sci. Lett. 473, 205–214. https://doi.org/10.1016/j.epsl.2017.06.011.
Morrill, C., Jacobsen, R.M., 2005. How widespread were climate anomalies 8200 years ago? Geophys. Res. Lett. 32, L19701. https://doi.org/10.1029/2005GL023536.
Morrill, C., Anderson, D.M., Bauer, B.A., Buckner, R., Gille, E.P., Gross, W.S., Hartman, M., Shah, A., 2013. Proxy benchmarks for intercomparison of 8.2 ka simulations. Clim. Past 9, 423–432. https://doi.org/10.5194/cp-9-423-2013.
Mosblech, N.A.S., Bush, M.B., Gosling, W.D., Hodell, D., Thomas, L., van Calsteren, P., Correa-Metrio, A., Valencia, B.G., Curtis, J., van Woesik, R., 2012. North Atlantic forcing of Amazonian precipitation during the last ice age. Nat. Geosci. 5, 817–820. https://doi.org/10.1038/ngeo1588.
Neff, U., Burns, S.J., Mangini, A., Mudelsee, M., Fleitmann, D., Matter, A., 2001. Strong coherence between solar variability and the monsoon in Oman between 9 and 6 kyr ago. Nature 411, 290–293. https://doi.org/10.1038/35077048.
Niedermeyer, E.M., Schefuß, E., Sessions, A.L., Mulitza, S., Mollenhauer, G., Schulz, M., Wefer, G., 2010. Orbital- and millennial-scale changes in the hydrologic cycle and vegetation in the western African Sahel: insights from individual plant wax δD and δ13C. Quat. Sci. Rev. 29, 2996–3005. https://doi.org/10.1016/j.quascirev.2010.06.039.
Novello, V.F., Cruz, F.W., McGlue, M.M., Wong, C.I., Ward, B.M., Vuille, M., Santos, R.A., Jaqueto, P., Pessenda, L.C.R., Atorre, T., Ribeiro, L.M.A.L., Karmann, I., Barreto, E.S., Cheng, H., Edwards, R.L., Paula, M.S., Scholz, D., 2019. Vegetation and environmental changes in tropical South America from the last glacial to the Holocene documented by multiple cave sediment proxies. Earth Planet. Sci. Lett. 524, 115717 https://doi.org/10.1016/j.epsl.2019.115717.

O'Brien, S.R., Mayewski, P.A., Meeker, L.D., Meese, D.A., Twickler, M.S., Whitlow, S.I., 1995. Complexity of holocene climate as reconstructed from a Greenland Ice Core. Science 270, 1962–1964. https://doi.org/10.1126/science.270.5244.1962.

Park, J., Yi, S., Cheul Kim, J., Lee, E., Choi, J., 2019. Abrupt Holocene climate shifts in coastal East Asia, including the 8.2 ka, 4.2 ka, and 2.8 ka BP events, and societal responses on the Korean peninsula. Sci. Rep. 9, 10806. https://doi.org/10.1038/s41598-019-47264-8.

Partin, J.W., Cobb, K.M., Adkins, J.F., Clark, B., Fernandez, D.P., 2007. Millennial-scale trends in west Pacific warm pool hydrology since the Last Glacial Maximum. Nature 449, 452–455. https://doi.org/10.1038/nature06164.

Peltier, W.R., 2004. Global glacial isostasy and the surface of the Ice-Age Earth: The ICE-5G (VM2) model and GRACE. Annu. Rev. Earth Planet. Sci. 32, 111–149. https://doi.org/10.1146/annurev.earth.32.082503.144359.

Rahmstorf, S., Box, J., Feulner, G., Mann, M.E., Robinson, A., Rutherford, S., Schaffernicht, E.J., 2015. Exceptional twentieth-century slowdown in Atlantic Ocean overturning circulation. Nat. Clim. Chang. 5, 475–480. https://doi.org/10.1038/nclimate2554.

Renssen, H., Goosse, H., Fichefet, T., Campin, J.M., 2001. The 8.2 kyr BP event simulated by a global atmosphere-sea-ice-ocean model. Geophys. Res. Lett. 28, 1567–1570. https://doi.org/10.1029/2000GL012602.

Shakun, J.D., Clark, P.U., He, F., Marcott, S.A., Mix, A.C., Liu, Z., Otto-Bliesner, B., Schmittner, A., Bard, E., 2012. Global warming preceded by increasing carbon dioxide concentrations during the last deglaciation. Nature 484, 49–54. https://doi.org/10.1038/nature10915.

Shanahan, T.M., McKay, N.P., Hughen, K.A., Overpeck, J.T., Otto-Bliesner, B., Heil, C.W., King, J., Scholz, C.A., Peck, J., 2015. The time-transgressive termination of the African Humid Period. Nat. Geosci. 8, 140–144. https://doi.org/10.1038/ngeo2329.

Shi, J., Yan, Q., 2019. Evolution of the Asian–African monsoonal precipitation over the last 21 kyr and the associated dynamic mechanisms. J. Clim. 32, 6551–6569. https://doi.org/10.1175/JCLI-D-19-0074.1.

Srokosz, M.A., Bryden, H.L., 2015. Observing the Atlantic meridional overturning circulation yields a decade of inevitable surprises. Science 348, 1255575 (doi: 110.1126/science.1255575).

Staubwasser, M., Sirocko, F., Grootes, P.M., Segl, M., 2003. Climate change at the 4.2 ka BP termination of the Indus valley civilization and Holocene south Asian monsoon variability. Geophys. Res. Lett. 30, 1425. https://doi.org/10.1029/2002GL016822.

Strikis, N.M., Cruz, F.W., Cheng, H., Karmann, I., Edwards, R.L., Vuille, M., Wang, X., de Paula, M.S., Novello, V.F., Auler, A.S., 2011. Abrupt variations in South American monsoon rainfall during the Holocene based on a speleothem record from central-eastern Brazil. Geology 39, 1075–1078. https://doi.org/10.1130/G32098.1.

Tan, L., Li, Y., Wang, X., Cai, Y., Lin, F., Cheng, H., Ma, L., Ashish, A., Edwards, R.L., 2020. Holocene monsoon change and abrupt events on the Western Chinese Loess Plateau as revealed by accurately dated stalagmites. Geophys. Res. Lett. 47 https://doi.org/10.1029/2020GL090273 e2020GL090273.

Tierney, J.E., Russell, J.M., Huang, Y., Damste, J.S.S., Hopmans, E.C., Cohen, A.S., 2008. Northern hemisphere controls on tropical Southeast African climate during the Past 60,000 years. Science 322, 252–255. https://doi.org/10.1126/science.1160485.

Tierney, J.E., Oppo, D.W., LeGrande, A.N., Huang, Y., Rosenthal, Y., Linsley, B.K., 2012. The influence of Indian Ocean atmospheric circulation on Warm Pool hydroclimate during the Holocene epoch. J. Geophys. Res. 117, D19108. https://doi.org/10.1029/2012JD018060.

Tierney, J.E., deMenocal, P.B., Zander, P.D., 2017a. A climatic context for the out-of-Africa migration. Geology 45, 1023–1026. https://doi.org/10.1130/G39457.1.

Tierney, J.E., Pausata, F.S.R., deMenocal, P.B., 2017b. Rainfall regimes of the Green Sahara. Sci. Adv. 3, e1601503 https://doi.org/10.1126/sciadv.1601503.

Tjallingii, R., Claussen, M., Stuut, J.-B.W., Fohlmeister, J., Jahn, A., Bickert, T., Lamy, F., Röhl, U., 2008. Coherent high- and low-latitude control of the northwest African hydrological balance. Nat. Geosci. 1, 670–675. https://doi.org/10.1038/ngeo289.

Trenberth, K.E., 1998. Atmospheric moisture residence times and cycling: implications for rainfall rates and climate change. Clim. Chang. 39, 667–694. https://doi.org/10.1023/A:1005319109110.

Trenberth, K.E., Stepaniak, D.P., Caron, J.M., 2000. The global monsoon as seen through the divergent atmospheric circulation. J. Clim. 13, 3969–3993. https://doi.org/10.1175/1520-0442(2000)013<3969:TGMAST>2.0.CO;2.

van Breukelen, M.R., Vonhof, H.B., Hellstrom, J.C., Wester, W.C.G., Kroon, D., 2008. Fossil dripwater in stalagmites reveals Holocene temperature and rainfall variation in Amazonia. Earth Planet. Sci. Lett. 275, 54–60. https://doi.org/10.1016/j.epsl.2008.07.060.

Voarintsoa, N.R.G., Matero, I.S.O., Railsback, L.B., Gregoire, L.J., Tindall, J., Sime, L., Cheng, H., Edwards, R.L., Brook, G.A., Kathayat, G., Li, X., Rakotondrazafy, A.F.M., Razanatseheno, M.O.M., 2019. Investigating the 8.2 ka event in northwestern Madagascar: Insight from data–model comparisons. Quat. Sci. Rev. 204, 172–186. https://doi.org/10.1016/j.quascirev.2018.11.030.

Wagner, A.J., Morrill, C., Otto-Bliesner, B.L., Rosenbloom, N., Watkins, K.R., 2013. Model support for forcing of the 8.2 ka event by meltwater from the Hudson Bay ice dome. Clim. Dyn. 41, 2855–2873. https://doi.org/10.1007/s00382-013-1706-z.

Walker, M., Head, M.J., Berkelhammer, M., Björck, S., Cheng, H., Cwynar, L., Fisher, D., Gkinis, V., Long, A., Lowe, J., Newnham, R., Rasmussen, S.O., Weiss, H., 2018. Formal ratification of the subdivision of the Holocene Series/Epoch (Quaternary System/Period): two new Global Boundary Stratotype Sections and Points (GSSPs) and three new stages/subseries. Episodes 41, 213–223. https://doi.org/10.18814/epiiugs/2018/018016.

Wang, B., Ding, Q., 2008. Global monsoon: Dominant mode of annual variation in the tropics. Dyn. Atmos. Oc. 44, 165–183. https://doi.org/10.1016/j.dynatmoce.2007.05.002.

Wang, Y., Cheng, H., Edwards, R.L., Kong, X., An, Z., Wu, J., Kelly, M.J., Dykoski, C.A., 2005. The holocene Asian monsoon: links to solar changes and North Atlantic climate. Science 308, 854–857. https://doi.org/10.1126/science.1106296.

Wang, B., Liu, J., Kim, H.-J., Webster, P.J., Yim, S.-Y., 2012. Recent change of the global monsoon precipitation (1979–2008). Clim. Dyn. 39, 1123–1135. https://doi.org/10.1007/s00382-011-1266-z.

Wang, B., Liu, J., Kim, H.-J., Webster, P.J., Yim, S.-Y., Xiang, B., 2013. Northern Hemisphere summer monsoon intensified by mega-El Niño/southern oscillation and Atlantic multidecadal oscillation. Proc. Natl. Acad. Sci. U. S. A. 110, 5347–5352. https://doi.org/10.1073/pnas.1219405110.

Wang, X., Edwards, R.L., Auler, A.S., Cheng, H., Kong, X., Wang, Y., Cruz, F.W., Dorale, J. A., Chiang, H.-W., 2017. Hydroclimate changes across the Amazon lowlands over the past 45,000 years. Nature 541, 204–207. https://doi.org/10.1038/nature20787.

Wang, B., Jin, C., Liu, J., 2020. Understanding future change of global monsoons projected by CMIP6 models. J. Clim. 33, 6471–6489. https://doi.org/10.1175/JCLI-D-19-0993.1.

Weldeab, S., Schneider, R.R., Kölling, M., Wefer, G., 2005. Holocene African droughts relate to eastern equatorial Atlantic cooling. Geology 33, 981. https://doi.org/10.1130/G21874.1.

Weldeab, S., Lea, D.W., Schneider, R.R., Andersen, N., 2007. 155,000 years of West African monsoon and ocean thermal evolution. Science 316, 1303–1307. https://doi.org/10.1126/science.1140461.

Weldeab, S., Lea, D.W., Oberhänsli, H., Schneider, R.R., 2014. Links between southwestern tropical Indian Ocean SST and precipitation over southeastern Africa over the last 17kyr. Palaeogeogr. Palaeoclimatol. Palaeoecol. 410, 200–212. https://doi.org/10.1016/j.palaeo.2014.06.001.

Wiersma, A.P., Renssen, H., Goosse, H., Fichefet, T., 2006. Evaluation of different freshwater forcing scenarios for the 8.2 ka BP event in a coupled climate model. Clim. Dyn. 27, 7–8. https://doi.org/10.1007/s00382-006-0166-0.

Winter, A., Zanchettin, D., Lachniet, M., Vieten, R., Pausata, F.S.R., Ljungqvist, F.C., Cheng, H., Edwards, R.L., Miller, T., Rubinetti, S., Rubino, A., Taricco, C., 2020. Initiation of a stable convective hydroclimatic regime in Central America circa 9000 years BP. Nat. Commun. 11, 716. https://doi.org/10.1038/s41467-020-14490-y.

Xie, P., Arkin, P.A., 1997. Global precipitation: A 17-year monthly analysis based on gauge observations, satellite estimates, and numerical model outputs. Bull. Am. Meteor. Soc. 78, 2539–2558. https://doi.org/10.1175/1520-0477(1997)078<2539:GPAYMA>2.0.CO;2.

Yan, M., Wang, B., Liu, J., 2016. Global monsoon change during the Last Glacial Maximum: a multi-model study. Clim. Dyn. 47, 359–374. https://doi.org/10.1007/s00382-015-2841-5.

Yan, M., Liu, Z., Ning, L., Liu, J., 2020. Holocene EASM-EAWM relationship across different timescales in CCSM3. Geophys. Res. Lett. 47 https://doi.org/10.1029/2020GL088451 e2020GL088451.

Yang, Y.-M., An, S.-I., Wang, B., Park, J.H., 2020. A global-scale multidecadal variability driven by Atlantic multidecadal Oscillation. Natl. Sci. Rev. 7, 1190–1197. https://doi.org/10.1093/nsr/nwz216.